Hybrid 2D [Pb(CH3NH2)I2]n coordination polymer precursor for scalable perovskite deposition

Febriansyah, Benny; Koh, Teck Ming; Rana, Prem Jyoti Singh; Hooper, Thomas James Nelson; Ang, Zhi Zhong; Li, Yongxin; Bruno, Annalisa; Grätzel, Michael; England, Jason; Mhaisalkar, Subodh Gautam; Mathews, Nripan

2020

Febriansyah, B., Koh, T. M., Rana, P. J. S., Hooper, T. J. N., Ang, Z. Z., Li, Y., ... Mathews, N. (2020). Hybrid 2D [Pb(CH3NH2)I2]n coordination polymer precursor for scalable perovskite deposition. ACS Energy Letters, 5(7), 2305–2312. doi:10.1021/acsenergylett.0c00781

Hybrid 2D $[Pb(CH_3NH_2)I_2]_n$ coordination polymer precursor for scalable perovskite deposition

Benny Febriansyah,[1,2,3] Teck Ming Koh,[1] Prem Jyoti Singh Rana,[1] Thomas J. N. Hooper,[1] Zhi Zhong Ang,[3] Yongxin Li,[3] Annalisa Bruno,[1] Michael Grätzel,[4] Jason England,[3] Subodh G. Mhaisalkar,[1,5] and Nripan Mathews.[1,5,]*

[1]Energy Research Institute at Nanyang Technological University (ERI@N), Research Techno Plaza, X-Frontier Block Level 5, 50 Nanyang Drive, Singapore 637553, Singapore.

[2]Interdiscipinary Graduate School (IGS), 50 Nanyang Avenue, Singapore 639798 Singapore.

[3]Division of Chemistry and Biological Chemistry, School of Physical and Mathematical Sciences, Nanyang Technological University, 21 Nanyang Link, Singapore 637371, Singapore.

[4]Laboratory of Photonics and Interfaces, Department of Chemistry and Chemical Engineering, Swiss Federal Institute of Technology, Station 6, Lausanne 1015, Switzerland.

[5]School of Materials Science and Engineering, Nanyang Technological University, 50 Nanyang Avenue, Singapore 639798, Singapore.

AUTHOR INFORMATION

Corresponding Author

*Correspondence: nripan@ntu.edu.sg

ABSTRACT. A two-dimensional hybrid coordination polymer $[Pb(CH_3NH_2)I_2]_n$ featuring a well-defined layered structure is reported for scalable perovskite ink and deposition. This coordination polymer exhibits structural, spectroscopic, and physicochemical properties distinct from common PbI_2 perovskite precursors. Notably, it serves as a methylamine "gas carrier" capable of liberating methylamine (CH_3NH_2) into the precursor solution, thus improving the solubility of perovskite in unconventional, greener processing solvents, such as acetonitrile. The purity of $[Pb(CH_3NH_2)I_2]_n$ single crystals and the ability of the precursor to reduce sources of defects such as polyiodide species in solution allow the formation of high quality perovskite films. This eventually results in efficient and stable devices, fabricated *via* single step anti-solvent-free deposition method, transferable to large-area slot die coating. Gram scale synthesis of this unique lead precursor is demonstrated, essential for the scale-up of perovskite photovoltaic technology.

TOC GRAPHICS

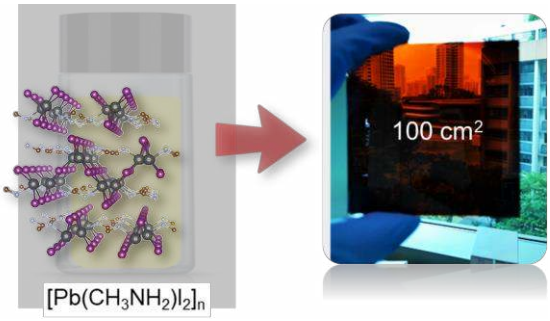

Since the first report as a solar absorber in 2009,[1] three-dimensional (3D) halide perovskites have experienced a meteoric rise, resulting in solar cells of over 25% certified power conversion efficiency (PCE).[2] Coupled with solution-based low-cost fabrication methodologies, such a rise has been made possible by the confluence of good optoelectronic properties, such as a suitable bandgap, large absorption coefficient,[3] low exciton binding energies,[4] long electron and hole diffusion lengths[5] with sufficient mobilities,[6] and absence of deep traps in the bandgap.[3] As a consequence, after less than a decade of intense research, halide perovskite solar cells are being evaluated as a viable technological alternative.[7-8] This tremendous progress has, however, been accompanied by the use of strongly coordinating, high boiling point solvents such as dimethylformamide (DMF), dimethylsulfoxide (DMSO), γ-butyrolactone (GBL) and *N*-Methyl-2-pyrrolidone (NMP),[9-13] which could become a major barrier to large scale manufacturing owing to the solvent handling and toxicology issues associated with them.[14-15]

Various scalable processing techniques have been explored to achieve uniform and high-quality perovskite films. Zhu and co-workers,[10] for example, demonstrated additive engineering and solvent tuning of the perovskite precursor ink which enabled a wide precursor-processing window and a rapid grain growth rate. Coupled with anti-solvent extraction process, the method was able to deliver perovskite films with large-scale uniformity. Utilizing different strategy, Tarasov and co-workers[16] showed perovskite conversion via polyiodide melts route where they employed a nanoscale layer of metallic Pb coated with stoichiometric amounts of iodide salts before subsequent exposure to iodine vapor. The instantly formed polyiodide liquid converts the Pb layer into perovskite films coated on big area substrates.

Apart from the two routes, deposition processes involving CH_3NH_2 gas have also been reported.[17-18] Such approach is particularly appealing because not only does CH_3NH_2 improve

the perovskite solubility in unconventional greener solvents, such as acetonitrile (ACN) and tetrahydrofuran (THF),[19-20] but it can also enhance the quality of the perovskite layers being fabricated. For example, Qi and co-workers[21] reported a scalable fabrication method of methylammonium lead iodide perovskite ($MAPbI_3$) by sequentially exposing the pre-formed lead iodide (PbI_2) thin films with CH_3NH_2 and hydroiodic (HI) vapors. It was shown that such a gas-induced reaction enabled the successful preparation of smooth and uniform perovskite films. Han and co-workers[22] further showed that prolonged exposure of PbI_2 and methyl ammonium iodide (MAI) with CH_3NH_2 gas, resulted in complexes of PbI_2:CH_3NH_2 and MAI:3CH_3NH_2, in paste and liquid forms, respectively. CH_3NH_2 gas was found to be easily released from the resulting complexes at low temperature (<50°C) because they were, presumably, formed as a result of weak intermolecular interactions between CH_3NH_2 and PbI_2 or MAI. Nonetheless, mixing of the two species eventually yielded "liquified" $MAPbI_3$ that could be deposited in large-area substrates. Very recently, similar method was demonstrated by Park and co-workers[20] where pre-grown $MAPbI_3$ single crystals were exposed to CH_3NH_2 gas to undergo "pseudoliquefaction *via* physisorption". Further dissolution of the liquified crystals in ACN then made it possible for perovskite deposition using D-bar coating method.

All the aforementioned precedent reports, nonetheless, have relied on PbI_2 as the perovskite precursor material.[19-22] Furthermore, despite evidence pointing to the positive effect of CH_3NH_2 in perovskite fabrication, the ability of this organic molecule to coordinate with Pb^{2+} has not been explored for the development of new perovskite precursors. Since PbI_2 is sparingly or completely insoluble in weakly-coordinating solvents,[23] this posits a major problem to the utilization of unconventional solvents in perovskite fabrication. As a result, large quantity of perovskite precursor ink preparation in such solvent systems has been rarely demonstrated.

We propose that the aforementioned problem can be addressed by exploiting the coordination chemistry of the CH_3NH_2 gas itself. In principle, due to the basicity of the amine group, it is feasible for CH_3NH_2 molecule to bind (i.e. form covalent bond as opposed to weak intermolecular interaction) to Lewis-acidic Pb^{2+} metal center, leading to a possible formation of a new class of compound. Indeed, this is what has been observed in other systems: hybrid polymeric adducts of PbI_2 with coordinating solvents DMF and DMSO (dimethylsulfoxide) have been isolated and identified as key intermediates of the perovskite crystallization.[24-25] As such, we postulate that the incorporation of CH_3NH_2 into the PbI_2 structure through formation of covalent bond should be achievable under certain condition, leading to "trapping" of this gas molecule in the iodoplumbate lattice. Following that, we then prepared concentrated solutions of PbI_2 and MAI in a mixture of CH_3NH_2, ethanol, and ethyl acetate under inert condition (see SI for details) to initiate the reaction between CH_3NH_2 and $[PbI_6]^{4-}$. Leaving the solutions standing for at least 24 h, free from disturbances, eventually resulted in big yellow colored single crystals with reasonable yield (over 70% relative to Pb^{2+}.)

X-ray crystallographic analysis of the compound formed, $[Pb(CH_3NH_2)I_2]_n$, yielded a well-defined structure displayed in **Figure 1a**. (See SI for the associated crystallographic, refinement data and a more detailed discussion of its crystal structures.) The compound features two-dimensional (2D) "corrugated" polymeric layers that comprises $[Pb(CH_3NH_2)I_4]^{-2}$ monomers. The Pb^{2+} ions therein are five coordinate and the resulting square pyramids connect to one another *via* the bridging I^- ions in edge- and vertex-sharing fashions. Such coordination geometry exhibited by Pb^{2+} in $[Pb(CH_3NH_2)I_2]_n$ is very rare and we are aware of only 1 precedent report of hybrid lead iodide-based coordination polymer exhibiting similar geometry (out of the more than 60 examples reported in the Cambridge Structural Database.)[26] The more common six coordinate

are found, for examples, in coordination complexes of iodoplumbates with DMF, DMSO, or pyridines.[24-25, 27-28] This newly formed single crystalline compound is termed $[Pb(CH_3NH_2)I_2]_n$ in order to highlight its continuous 2D structure and to differentiate it from other discrete lead-centered coordination complexes that have been published earlier.[29-31]

Our compound also represents the first example of organoiodoplumbate coordination polymer where monoamine is used as the organic ligand. CH_3NH_2 coordinates strongly to the metal center with Pb-N bond distance being 2.452 Å. Such strong coordination of the amine functionality is accentuated by the thermal stability of the complex. As shown in thermal gravimetric analysis (TGA) plot of $[Pb(CH_3NH_2)I_2]_n$, degradation corresponding to the release of CH_3NH_2 gas does not occur up to 100°C (**Figure S1**). The $[Pb(CH_3NH_2)I_2]_n$ single crystals can be obtained in high purity (see SI for elemental analysis) and most importantly, it can be isolated in a big amount as a bulk. **Figure S2** shows of around 25 g of isolated $[Pb(CH_3NH_2)I_2]_n$. The purity of resulting bulk is further confirmed using powder X-ray diffraction (PXRD) carried out under inert condition. As shown in **Figure 1b**, the PXRD pattern of synthesized crystalline $[Pb(CH_3NH_2)I_2]_n$ is well in agreement with the material's simulated RT PXRD pattern.

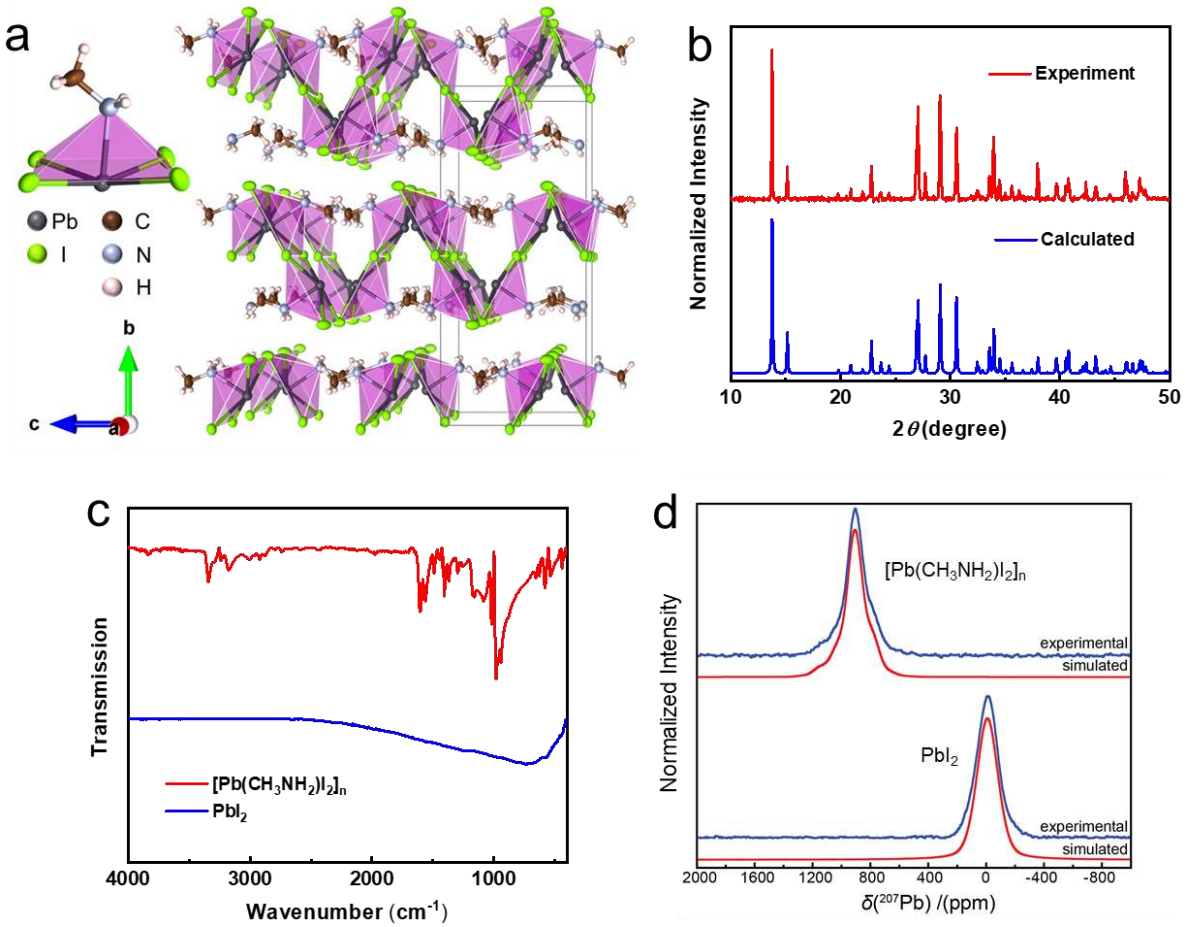

Figure 1. a) Single crystal X-ray structure of "2D" organometallic polymer $[Pb(CH_3NH_2)I_2]_n$ as viewed along the a-direction. Ellipsoids are shown at 50% probability. b) PXRD patterns of bulk $[Pb(CH_3NH_2)I_2]_n$ at RT. For comparison, the simulated RT PXRD pattern is included. Further XRD patterns comparison between bulk $[Pb(CH_3NH_2)I_2]_n$ and those calculated for PbI_2, MAI, and $MAPbI_3$ are presented in **Figure S14**. c) FT-IR spectrum of $[Pb(CH_3NH_2)I_2]_n$ (top) in comparison to that of PbI_2 (bottom). d) ^{207}Pb solid-state NMR spectra of $[Pb(CH_3NH_2)I_2]_n$ (top) and PbI_2 (bottom), under MAS frequencies of 15 and 12 KHz respectively, alongside their simulated line-shapes.

As a result of coordination of CH_3NH_2 to Pb-I lattices, our compound exhibits spectroscopic features that are distinctive to those of the more commonly used perovskite precursor, PbI_2. For example, due to the presence of CH_3NH_2, organic fingerprint can noticeably be observed in $[Pb(CH_3NH_2)I_2]_n$ from its Fourier-transform infrared (FT-IR) spectrum, a feature that is otherwise absent in PbI_2 (**Figure 1c**). The differing coordination environments of Pb in $[Pb(CH_3NH_2)I_2]_n$ in comparison to PbI_2, can also be discerned using solid-state (SS) NMR measurements (**Figure 1d**). Particularly, the ^{207}Pb SSNMR spectrum of $[Pb(CH_3NH_2)I_2]_n$ contains a single resonance at 905 ppm, whereas that of ^{207}Pb in PbI_2 falls at -10 ppm.[32-33] In addition, unlike PbI_2 which exhibits a Gaussian-shape resonance, asymmetry in its line-shape can be observed in that of $[Pb(CH_3NH_2)I_2]_n$ as a result of the reduced symmetry about its Pb atom coordination geometry, in comparison to the octahedral Pb-I configurations in PbI_2. (See SI for further discussion and details regarding SSNMR features of $[Pb(CH_3NH_2)I_2]_n$.) Variation in the spectroscopic properties is also apparent with organic CH_3NH_2 in $[Pb(CH_3NH_2)I_2]_n$. As can be seen in its ^{13}C SSNMR spectrum, a single resonance, owing to the methyl functionality, at 35 ppm is yielded (**Figure S3**). Such resonance has a distinct chemical environment in comparison to that in MAI where resonance at 29 has been reported.[34-35] The downfield shift suggests that, relative to ammonium group, the bonding with Pb^{+2} by the N atom results in a more withdrawing environment for the C atom in CH_3 functionality.

In order to exploit the "trapped" CH_3NH_2, we then utilized $[Pb(CH_3NH_2)I_2]_n$ as the precursor to fabricate perovskites utilising weakly coordinating solvents such as ACN. A black suspension was obtained with MAI and PbI_2 in ACN solvent, even with concentration as low as 100 mM. Intriguingly, in comparison to conventional PbI_2, the presence of extra CH_3NH_2 gas molecule originating from $[Pb(CH_3NH_2)I_2]_n$ precursor is found to increase the perovskite solubility. As

shown in **Figure 2a**, a clear solution could be obtained by mixing $[Pb(CH_3NH_2)I_2]_n$ and MAI in ACN. As such, $[Pb(CH_3NH_2)I_2]_n$ can be seen as the "CH_3NH_2 gas carrier" that is capable of liberating CH_3NH_2 upon dissolution. The $[Pb(CH_3NH_2)I_2]_n$ precursor was also found to be capable of improving the perovskite solubility when we attempted to introduce more CH_3NH_2 gas into suspensions containing $[Pb(CH_3NH_2)I_2]_n$ and MAI (see SI for details) with molar concentration higher than 100 mM.[19] In particular, we observed a much faster dissolution process in comparison to when PbI_2 was used as a precursor. This observation became more apparent when higher concentration or huge amount of solution was used. For example, with our set-up, in order to dissolve 0.50 M of 35 mL of solution, typically 5 hours are required to get clear solution with PbI_2 and MAI starting precursors. Replacing PbI_2 with $[Pb(CH_3NH_2)I_2]_n$, by maintaining the flow and stirring rate for equal comparison, the dissolution time was reduced to around 1.5 hours (**Figure S4**). This, as mentioned previously, can be attributed to the extra CH_3NH_2 molecule that is "carried" by the compound (**Figure 2b**).

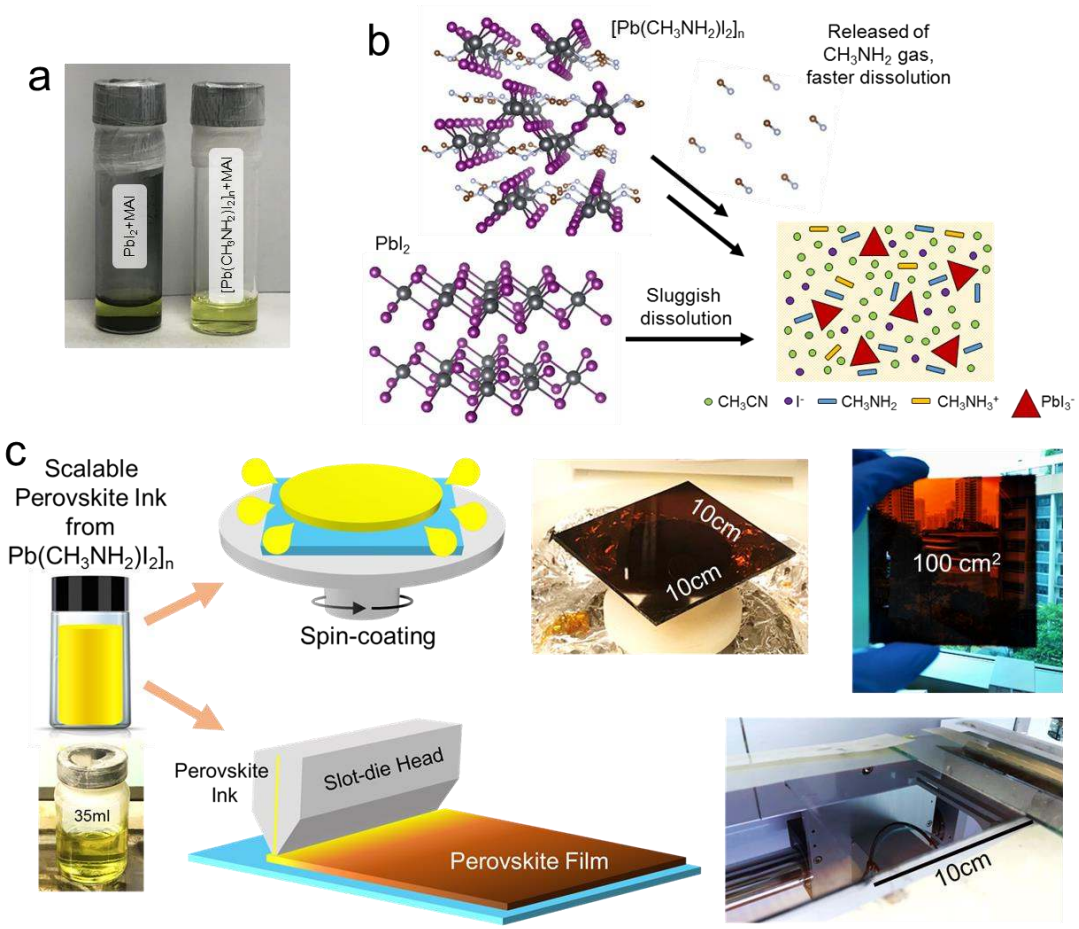

Figure 2. a) Vials of perovskite precursors CH_3NH_3I : PbI_2 (1 : 1 molar ratio) in ACN (left, 100 mM), and CH_3NH_3I : $[Pb(CH_3NH_2)I_2]_n$ (1 : 1 molar ratio) in ACN (right, 100 mM). b) Schematic illustration showing faster dissolution of CH_3NH_3I : $[Pb(CH_3NH_2)I_2]_n$ in ACN due to release of CH_3NH_2 gas carried by $[Pb(CH_3NH_2)I_2]_n$. c) Schematic illustrations for spin coating and slot-die coating perovskite deposition processes using precursor ink containing $[Pb(CH_3NH_2)I_2]_n$, along with the photographs of the resulting $MAPbI_3$ films deposited on 10 × 10 cm^2 substrates.

The ability of our compound to provide faster solubilization of perovskite eventually allowed us to prepare sufficient amount of ink needed for fabrication of large perovskite films, such as

via spin- and slot-die coating processes (**Figure 2c; Movies S1 and S2**). Coupled with the fast evaporation of the solvent, perovskite films featuring fully covered, pin-holes-free, uniform morphology can be obtained on large area substrate at room temperature without the need of anti-solvent (**Figures 2c and 3a**). Specifically, glancing-angle X-ray diffraction (GAXRD) and UV-vis absorption carried out on slot-die coated large area films that are divided into eight smaller samples, suggest the homogeneity of the perovskite layer fabricated (**Figure S5**). On the contrary, under the same experimental parameters (see SI), very thin and opaque films were typically obtained from perovskite ink composed mainly of DMF as the solvent (**Figure S6**). This points to the importance of low boiling point and low coordinating capability of ACN in forming high quality perovskite at ambient condition. Thus, we foresee a potential use of our compound for the scale-up of the perovskite ink when the required amount of ink is huge.

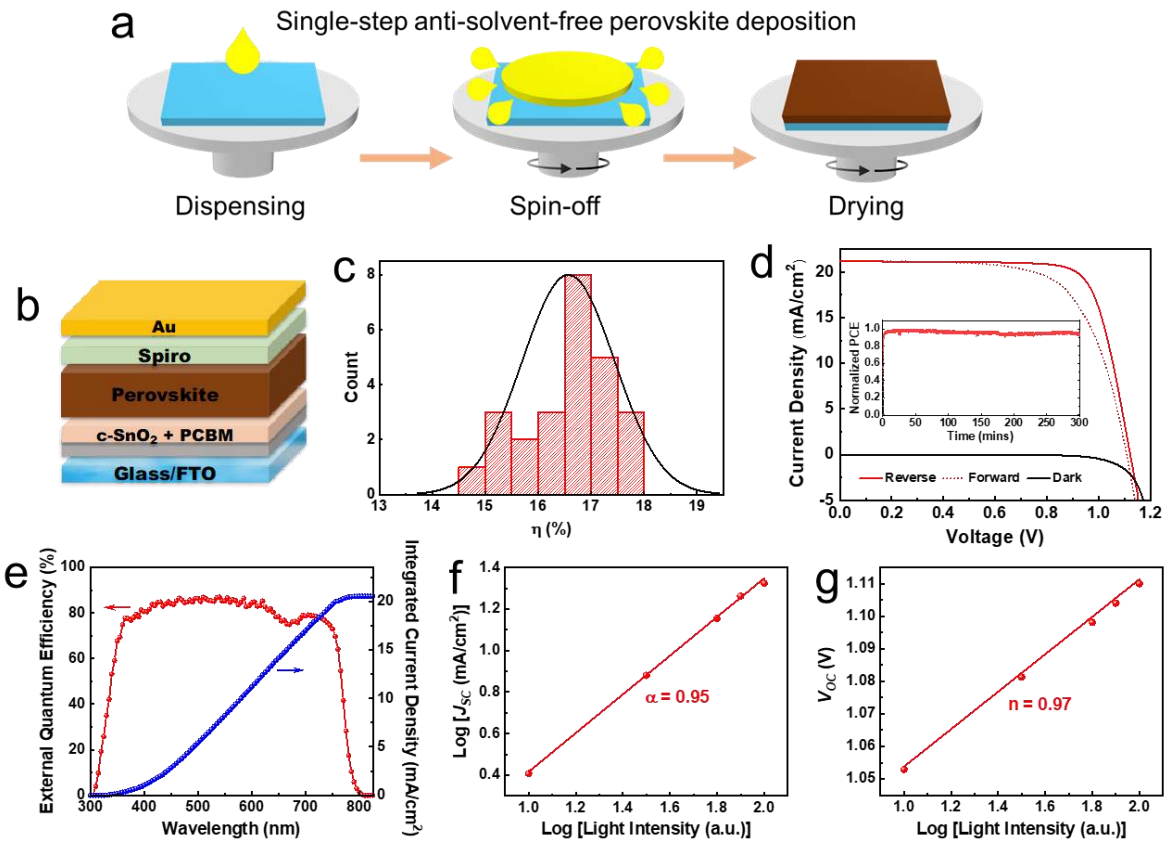

Figure 3. a) Schematic illustration of perovskite formation process based on precursor ink based on $[Pb(CH_3NH_2)I_2]_n$. b) Schematic diagram of the planar perovskite solar cell structure implemented in our study fabricated *via* one-step, anti-solvent-free spincoating method. c) Power conversion efficiency distribution of solar cells fabricated from on precursor ink based on $[Pb(CH_3NH_2)I_2]_n$. d) *J-V* characteristics and e) IPCE spectrum and integrated current density of the best performing device fabricated from ink based on $[Pb(CH_3NH_2)I_2]_n$. Inset in the panel d shows MPP tracking under constant illumination of an unencapsulated device in nitrogen atmosphere at RT. Light-intensity-dependent of f) J_{SC} and g) V_{OC} behavior of corresponding best performing solar cell.

To evaluate the $[Pb(CH_3NH_2)I_2]_n$ precursor ink, fabrication of perovskite solar cells (*via* one-step, anti-solvent-free spincoating method) in an "n-i-p" configuration with planar tin oxide (SnO_2) electron- transporting layers and Spiro-OMeTAD hole transporter was carried out (**Figures 3a-b**, see SI for details). A very thin layer of [6,6]-phenyl-C61-butyric acid methyl ester (PCBM) was used as passivation layer at the interface between SnO_2 and perovskite, as previously reported.[36] Statistical representations of each photovoltaic parameter for the resultant 25 devices are depicted in **Figures 3c and S7**, which confirms the reproducibility of the device fabrication process. In particular, the devices fabricated with our perovskite ink yielded an average PCE of 16.60% with average open-circuit voltage (V_{OC}), short-circuit current density (J_{SC}), and fill-factor (FF) of 1.08 V, 20.38 mA cm^{-2}, and 75.08%, respectively, when measured under a simulated air mass (AM 1.5) of 1 sun illumination (100 mW cm^{-2}). Current density-voltage (*J-V*) characteristic of the best performing device is further presented in **Figure 3d**. V_{OC}, J_{SC}, and FF of 1.110 V, 21.16 mA/cm^2, and 0.77, respectively, are observed in the reverse scan direction, yielding to PCE of 18.00%, while V_{OC}, J_{SC}, and FF of 1.105 V, 21.21 mA/cm^2, and 0.74, respectively, are recorded in the forward scan direction, resulting in PCE of 17.21%. Maximum powerpoint tracking (MPPT) under constant light illumination was also performed over a period of 5 hours to obtain the stabilized efficiency of the fabricated device (**inset of Figure 3d**).

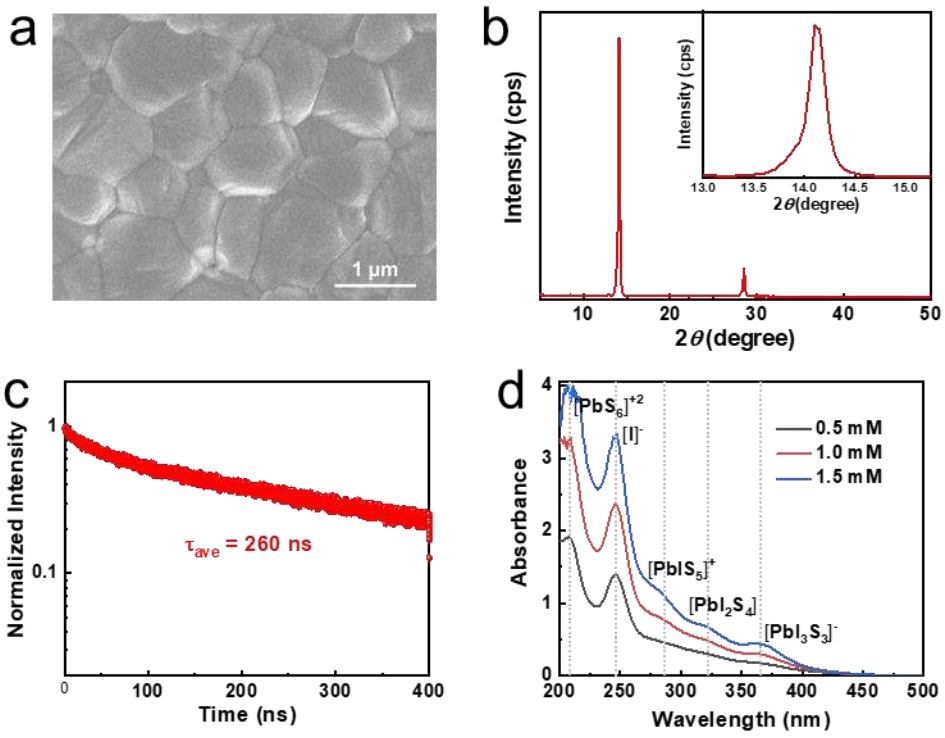

Figure 4. a) Surface morphology view of FE-SEM image of the perovskite films deposited from the precursor ink containing $[Pb(CH_3NH_2)I_2]_n$. b) GAXRD patterns of the fabricated perovskite film. Inset shows the (100) peak of 2θ = ca. 14.14°. c) Time-resolved PL decay spectra of the fabricated perovskite film. d) Absorption spectra of solutions containing CH_3NH_3I : $[Pb(CH_3NH_2)I_2]_n$ (1 : 1 molar ratio) in ACN in different concentrations. The experiments were kept at 1.5 mM to prevent saturation of the signal at high energy region, such that the ratio between each of the peaks can be discerned clearly. The assignment of the peaks is based on refs. [37-40].

Notably, the obtained efficiency figures are on par with $MAPbI_3$ devices fabricated from similar green solvent system where pristine PbI_2 was used as starting precursor (**Figure S8** and refs. 19-20, 41-43 for other reported works). This indicates that utilization of the as synthesized

$[Pb(CH_3NH_2)I_2]_n$ in the precursor ink does not compromise the overall device performance. The corresponding typical incident-to-photon-efficiency (IPCE) spectrum that shows an integrated J_{SC} of 20.52 mA/cm^2 is also shown in **Figure 3f**, which highlights the consistency of current density being obtained from our fabricated devices. The charge carrier recombination within the device was further investigated by measuring the light intensity dependent behavior (measured from 100 to 10 mW cm^{-2}) of the device's J_{SC} and V_{OC}. The power law dependence profile of J_{SC} with light intensity ($J_{SC} \propto I^{\alpha}$, with I and α being the light intensity and the exponential factor, respectively) of the device is presented in **Figure 3f**. Typically, good perovskite solar cells with no space charge effects show an α value close to 1, which indicates charge collection efficiency was independent of light intensity.[44] The device fabricated from our precursor ink displayed a slope of ca. 0.95, suggesting good perovskite crystal quality, reduced nonradiative recombination and efficient carrier collection in our solar cell. **Figure 3g** further shows the dependence of V_{OC} on the illuminated light intensity (I). The diode ideality factor (n) is employed to describe the dependence of the voltage on the applied light intensity as illustrated by the following equation:

$$n = \frac{q}{2.303 k_B T} \times \frac{dV_{OC}}{d\,log(I)} \qquad (1)$$

where n, k_B, q, and T are ideality factor, Boltzmann's constant, elementary charge, and temperature, respectively. Generally, the fitted n values are located between 1-2, which represents Shockley-Read-Hall trap-assisted recombination.[45] In the present case, our device exhibits the n value of ca. 0.97, which suggests reduced trap-assisted recombination. This result is consistent with the conclusion from *J-V* curves where good V_{OC} of 1.11 V can be obtained.

The high efficiency device obtained from our precursor ink can be ascribed to facile perovskite crystallization in the absence of anti-solvent as well as the presence of CH_3NH_2 species in the solution which reduces the formation of defects. The crystalline nature of our perovskite films is evident from the corresponding scanning electron microscope (SEM) images and GAXRD pattern. As shown in **Figures 4a and S9**, our typical films feature uniform, compact perovskite crystallites with big grain sizes and of high crystallinity. In particular, densely packed crystal grains with an average size of ca. 700 nm are observed, together with strong and sharp (110) XRD peak with narrow full width at half maximum (FWHM) of ca. 0.181° (**Figure 4b**, inset). Additionally, our perovskite films exhibit a sharp absorption edge (**Figure S10, red curve**), narrow photoluminescence (PL) band with FWHM of ca. 40 nm (**Figure S10, blue curve**), and relatively long PL lifetime of 260 ns (**Figure 4c**). Such feature can be correlated to the reduced density of defects owing to the presence of CH_3NH_2 molecule which is expected to reduce polyiodide species in solution.[46] From optical absorption spectra of different concentrations of $[Pb(CH_3NH_2)I_2]_n$ and MAI solution in ACN, the peak attributed to $[PbI_3S_3]^-$, where S is coordinating species, (CH_3NH_2 in our case; see **Figure S11** for solution state NMR analysis of CH_3NH_2 binding), at ca. 370 nm[37, 46] appears at a very low intensity relative to the other peaks (**Figure 4d**). From mass spectrometry, it was also found that the relative amount of $[PbI_3]^-$ species (m/z = ca. 588.70) is much lower in comparison to that of I^- (m/z = ca. 126.89; see **Figure S12**). We believe this ability of CH_3NH_2 to suppress the polyiodide species in solution is crucial for the formation of high quality perovskite film from any green noncoordinating solvents.

In summary, we report for the first time the synthesis, isolation and characterizations of unprecedented $[Pb(CH_3NH_2)I_2]_n$ that features 2D structure. It is a well-defined compound which has distinctive structural, spectroscopic, and physicochemical properties from commonly used perovskite precursor, PbI_2. Notably, it serves as a CH_3NH_2 "gas carrier" capable of liberating CH_3NH_2 into precursor solution upon dissolution, thus improving the solubility of perovskite in unconventional, relatively greener processing solvent, such as acetonitrile. The purity of the isolated $[Pb(CH_3NH_2)I_2]_n$ and the ability of CH_3NH_2 to reduce sources of defects such as iodine or polyiodide species in solution allow the formation of high quality perovskite films. This eventually results in devices with power conversion efficiency of up to 18%, fabricated *via* single step anti-solvent-free deposition method.

Most importantly, this unique lead precursor can easily be prepared in a bulk and as such, is beneficial for preparation of large quantity perovskite ink in unconventional solvent, which is essential for commercial practice in scaling-up of perovskite photovoltaic technology. Future avenues of research includes exploration and optimization of alternative synthetic routes to $[Pb(CH_3NH_2)I_2]_n$,. Another avenue is directed toward synthetic development of the formamidine ($HN=CHNH_2$) variant of the material (i.e. $[Pb(HN=CHNH_2)I_2]_n$). It is envisioned that the availability of both $[Pb(CH_3NH_2)I_2]_n$ and hypothetical $[Pb(HN=CHNH_2)I_2]_n$ would be of high value as they can serve as starting precursors for mixed A-site cation halide perovskites, which would provide access to highly efficient and more stable perovskite solar cells.

ASSOCIATED CONTENT

Supporting Information. Materials synthesis, experimental procedures, additional spectra and crystallographic details are given in the Supporting Information.

Document S1. Main supplemental PDF.

Video S1. Spin coating.

Video S2. Slot die coating.

Crystallographic information file (CIF) of $[Pb(CH_3NH_2)I_2]_n$.

Notes

The authors declare no competing interests. CIF data for associated crystal structures have been deposited in the Cambridge Crystallographic Data Centre under deposition numbers CCDC 1970220-1970221.

ACKNOWLEDGMENT

NM, SGM, BF, TMK, PJSR, TJNH, and AB would like to acknowledge funding from the Singapore National Research Foundation through the Intra-CREATE Collaborative Grant (NRF2018-ITC001-001), Office of Naval Research Global (ONRG-NICOP-N62909-17-1-2155) and the Competitive Research Program: NRF–CRP14–2014–03. JE thanks NTU for funding (M4081442).

DECLARATION OF INTERESTS

Two of the authors, N.M. and S.M., are directors of Prominence Photovoltaics Pte Ltd, a perovskite solar cell commercialization company. The other authors declare no competing interests.

REFERENCES

(1) Kojima, A.; Teshima, K.; Shirai, Y.; Miyasaka, T. Organometal halide perovskites as visible-light sensitizers for photovoltaic cells. *J. Am. Chem. Soc.* **2009**, *131*, 6050−6051.

(2) Best Research-Cell Efficiencies Rev. 6-11-2019 (NREL), 2019, https://www.nrel.gov/pv/assets/pdfs/best-research-cell-efficiencies.20191106.pdf.

(3) Yin, W.-J.; Shi, T.; Yan, Y. Unique properties of halide perovskites as possible origins of the superior solar cell performance. *Adv. Mater.* **2014,** *26* (27), 4653-4658.

(4) Miyata, A.; Mitioglu, A.; Plochocka, P.; Portugall, O.; Wang, J. T.-W.; Stranks, S. D.; Snaith, H. J.; Nicholas, R. J. Direct measurement of the exciton binding energy and effective masses for charge carriers in organic–inorganic tri-halide perovskites. *Nat. Phys.* **2015,** *11* (7), 582-587.

(5) Xing, G.; Mathews, N.; Sun, S.; Lim, S.S.; Lam, Y. M.; Graïzel, M.; Mhaisalkar, S.; Sum, T. C. Long-range balanced electron- and hole-transport lengths in organic-inorganic $CH_3NH_3PbI_3$. *Science* **2013**, *342*, 344−347.

(6) Chen, Y.; Yi, H. T.; Wu, X.; Haroldson, R.; Gartstein, Y. N.; Rodionov, Y. I.;

Tikhonov, K. S.; Zakhidov, A.; Zhu, X. Y.; Podzorov, V. Extended carrier lifetimes and diffusion in hybrid perovskites revealed by Hall effect and photoconductivity measurements. *Nat. Commun.* **2016,** *7*, 12253.

(7) Extance, A. The reality behind solar power's next star material. *Nature* **2019**, *570*, 429 - 432.

(8) Forgacs, D.; Wojciechowski, K.; Malinkiewicz, O., *Perovskite Photovoltaics: From Laboratory to Industry*. In *High-Efficient Low-Cost Photovoltaics: Recent Developments*; Petrova-Koch, V.; Hezel, R.; Goetzberger, A.; Springer: Cham, 2020; 219-249.

(9) Deng, Y.; Zheng, X.; Bai, Y.; Wang, Q.; Zhao, J.; Huang, J. Surfactant-controlled ink drying enables high-speed deposition of perovskite films for efficient photovoltaic modules. *Nat. Energy* **2018,** *3* (7), 560-566.

(10) Yang, M.; Li, Z.; Reese, M. O.; Reid, O. G.; Kim, D. H.; Siol, S.; Klein, T. R.; Yan, Y.; Berry, J. J.; van Hest, M. F. A. M.; Zhu, K. Perovskite ink with wide processing window for scalable high-efficiency solar cells. *Nat. Energy* **2017,** *2* (5), 17038.

(11) Mei, A.; Li, X.; Liu, L.; Ku, Z.; Liu, T.; Rong, Y.; Xu, M.; Hu, M.; Chen, J.; Yang, Y.; Grätzel, M.; Han, H. A hole-conductor-free, fully printable mesoscopic perovskite solar cell with high stability. *Science* **2014**, *345* (6194), 295-298.

(12) Min, H.; Kim, M.; Lee, S-U.; Kim, H.; Kim, G.; Choi, K.; Lee, J. H.; Seok, S. I. Efficient, stable solar cells by using inherent bandgap of α-phase formamidinium

lead iodide. *Science* **2019**, *366* (6466), 749-753.

(13) Jiang, Q.; Zhao, Y.; Zhang, X.; Yang, X.; Chen, Y.; Chu, Z.; Ye, Q.; Li, X.; Yin, Z.; You, J. Surface passivation of perovskite film for efficient solar cells. *Nat. Photonics* **2019,** *13* (7), 460-466.

(14) Gardner, K. L.; Tait, J. G.; Merckx, T.; Qiu, W.; Paetzold, U. W.; Kootstra, L.; Jaysankar, M.; Gehlhaar, R.; Cheyns, D.; Heremans, P.; Poortmans, J. Nonhazardous Solvent Systems for Processing Perovskite Photovoltaics. *Adv. Energy Mater.* **2016,** *6* (14), 1600386.

(15) Byrne, F. P.; Jin, S.; Paggiola, G.; Petchey, T. H. M.; Clark, J. H.; Farmer, T. J.; Hunt, A. J.; Robert McElroy, C.; Sherwood, J. Tools and techniques for solvent selection: green solvent selection guides. *Sustain. Chem. Process* **2016,** *4* (1), 7.

(16) Turkevych, I.; Kazaoui, S.; Belich, N. A.; Grishko, A. Y.; Fateev, S. A.; Petrov, A. A.; Urano, T.; Aramaki, S.; Kosar, S.; Kondo, M.; Goodilin, E. A.; Graetzel, M.; Tarasov, A. B. Strategic advantages of reactive polyiodide melts for scalable perovskite photovoltaics. *Nat Nanotechnol* **2019,** *14* (1), 57-63.

(17) Kim, D. H.; Whitaker, J. B.; Li, Z.; van Hest, M. F. A. M.; Zhu, K. Outlook and Challenges of Perovskite Solar Cells toward Terawatt-Scale Photovoltaic Module Technology. *Joule* **2018,** *2* (8), 1437-1451.

(18) Wang, P.; Wu, Y.; Cai, B.; Ma, Q.; Zheng, X.; Zhang, W. H. Solution-Processable Perovskite Solar Cells toward Commercialization: Progress and Challenges. *Adv. Funct. Mater.* **2019,** *29* (47), 1807661.

(19) Noel, N. K.; Habisreutinger, S. N.; Wenger, B.; Klug, M. T.; Hörantner, M. T.; Johnston, M. B.; Nicholas, R. J.; Moore, D. T.; Snaith, H. J. A low viscosity, low boiling point, clean solvent system for the rapid crystallisation of highly specular perovskite films. *Energy Environ. Sci.* **2017,** *10* (1), 145-152.

(20) Jeong, D.-N.; Lee, D.-K.; Seo, S.; Lim, S. Y.; Zhang, Y.; Shin, H.; Cheong, H.; Park, N.-G. Perovskite Cluster-Containing Solution for Scalable D-Bar Coating toward High-Throughput Perovskite Solar Cells. *ACS Energy Lett.* **2019,** *4* (5), 1189-1195.

(21) Raga, S. R.; Ono, L. K.; Qi, Y. Rapid perovskite formation by CH_3NH_2 gas-induced intercalation and reaction of PbI_2. *J. Mater. Chem. A* **2016,** *4* (7), 2494-2500.

(22) Chen, H.; Ye, F.; Tang, W.; He, J.; Yin, M.; Wang, Y.; Xie, F.; Bi, E.; Yang, X.; Gratzel, M.; Han, L. A solvent- and vacuum-free route to large-area perovskite films for efficient solar modules. *Nature* **2017,** *550* (7674), 92-95.

(23) Hamill, J. C.; Schwartz, J.; Loo, Y.-L. Influence of Solvent Coordination on Hybrid Organic–Inorganic Perovskite Formation. *ACS Energy Lett.* **2017,** *3* (1), 92-97.

(24) Guo, Y.; Shoyama, K.; Sato, W.; Matsuo, Y.; Inoue, K.; Harano, K.; Liu, C.; Tanaka, H.; Nakamura, E. Chemical Pathways Connecting Lead(II) Iodide and Perovskite via Polymeric Plumbate(II) Fiber. *J. Am. Chem. Soc.* **2015,** *137* (50), 15907-14.

(25) Cao, J.; Jing, X.; Yan, J.; Hu, C.; Chen, R.; Yin, J.; Li, J.; Zheng, N. Identifying the Molecular Structures of Intermediates for Optimizing the Fabrication of High-Quality Perovskite Films. *J. Am. Chem. Soc.* **2016,** *138* (31), 9919-26.

(26) Marandi, F.; Garousi, E.; Fun, H.-K. Supramolecular organization in lead(II) halides of 4,4′-dimethoxy-2,2′-bipyridine ligand. *J. Mol. Struct.* **2013,** *1049*, 205-211.

(27) Miyamae, H.; Toriyama, H.; Abe, T.; Hihara, G.; Nagata, M. The structure of PbI2-pyridine adducts. I. Lead(II) iodide-pyridine (2/4), catena-di-[μ]-iodo-bis(pyridine)lead(II), $[Pb_2I_4(C_5H_5N)_4]$. *Acta Cryst.* **1984,** C40, 1559-1562.

(28) Engelhardt, L. M.; Patrick, J. M.; Whitaker, C. R.; White, A. H. Lewis Base Adducts of Lead(II) Compounds. I. Polymer Isomerism in Some 1-2 Adducts of Lead(II) Halides With Pyridine Bases. *Aust. J. Chem.* **1987,** *40* (12), 2107-2114.

(29) Davidovich, R. L.; Stavila, V.; Marinin, D. V.; Voit, E. I.; Whitmire, K. H., Stereochemistry of lead(II) complexes with oxygen donor ligands. *Coord. Chem. Rev.* **2009,** *253* (9-10), 1316-1352.

(30) Parr, J. Some recent coordination chemistry of lead(II). *Polyhedron* **1997***, 16 (4),* 551-566.

(31) Leeper, R. W.; Summers, L.; Gilman, H. Organolead Compounds. *Chem. Rev.* **1954***, 54 (1)* 101-167.

(32) Bernard, G. M.; Wasylishen, R. E.; Ratcliffe, C. I.; Terskikh, V.; Wu, Q.; Buriak, J. M.; Hauger, T. Methylammonium Cation Dynamics in Methylammonium Lead Halide Perovskites: A Solid-State NMR Perspective. *J. Phys. Chem. A* **2018,** *122* (6), 1560-1573.

(33) Roiland, C.; Trippe-Allard, G.; Jemli, K.; Alonso, B.; Ameline, J. C.; Gautier,

R.; Bataille, T.; Le Polles, L.; Deleporte, E.; Even, J.; Katan, C. Multinuclear NMR as a tool for studying local order and dynamics in $CH_3NH_3PbX_3$ (X = Cl, Br, I) hybrid perovskites. *Phys. Chem. Chem. Phys.* **2016,** *18* (39), 27133-27142.

(34) Van Gompel, W. T. M.; Herckens, R.; Reekmans, G.; Ruttens, B.; D'Haen, J.; Adriaensens, P.; Lutsen, L.; Vanderzande, D. Degradation of the Formamidinium Cation and the Quantification of the Formamidinium–Methylammonium Ratio in Lead Iodide Hybrid Perovskites by Nuclear Magnetic Resonance Spectroscopy. *J. Phys. Chem. C* **2018,** *122* (8), 4117-4124.

(35) Baikie, T.; Barrow, N. S.; Fang, Y.; Keenan, P. J.; Slater, P. R.; Piltz, R. O.; Gutmann, M.; Mhaisalkar, S. G.; White, T. J. A combined single crystal neutron/X-ray diffraction and solid-state nuclear magnetic resonance study of the hybrid perovskites $CH_3NH_3PbX_3$ (X = I, Br and Cl). *J. Mater. Chem. A* **2015,** *3* (17), 9298-9307.

(36) Wang, J.; Datta, K.; Weijtens, C. H. L.; Wienk, M. M.; Janssen, R. A. J. Insights into Fullerene Passivation of SnO_2 Electron Transport Layers in Perovskite Solar Cells. *Adv. Func. Mater.* **2019,** *29* (46), 1905883.

(37) Rahimnejad, S.; Kovalenko, A.; Fores, S. M.; Aranda, C.; Guerrero, A. Coordination Chemistry Dictates the Structural Defects in Lead Halide Perovskites. *ChemPhysChem* **2016**, *17*, 2795 – 2798.

(38) Berghmans, F.; Mignani, A. G.; De Moor, P.; Tan, C. H.; Moo, Y. C.; Mat Jafri, M. Z.; Lim, H. S., UV spectroscopy determination of aqueous lead and copper ions in water. In *Optical Sensing and Detection III*, **2014**, *9141*, 91410N.

(39) Kireev, S. V.; Shnyrev, S. L. Study of molecular iodine, iodate ions, iodide ions, and triiodide ions solutions absorption in the UV and visible light spectral bands. *Laser Phys.* **2015,** *25* (7), 075602.

(40) Wei, Y. J.; Liu, C. G.; Mo, L. P., *Spectroscopy and Spectral Analysis*, **2005**, *25* (1), 86-88.

(41) Dou, B.; Whitaker, J. B.; Bruening, K.; Moore, D. T.; Wheeler, L. M.; Ryter, J.; Breslin, N. J.; Berry, J. J.; Garner, S. M.; Barnes, F. S.; Shaheen, S. E.; Tassone, C. J.; Zhu, K.; van Hest, M. F. A. M. Roll-to-Roll Printing of Perovskite Solar Cells. *ACS Energy Lett.* **2018,** *3* (10), 2558-2565.

(42) Uribe, J. I.; Ciro, J.; Montoya, J. F.; Osorio, J.; Jaramillo, F. Enhancement of Morphological and Optoelectronic Properties of Perovskite Films by CH_3NH_3Cl Treatment for Efficient Solar Minimodules. *ACS Appl. Energy Mater.* **2018,** *1* (3), 1047-1052.

(43) Ramadan, A. J.; Noel, N. K.; Fearn, S.; Young, N.; Walker, M.; Rochford, L. A.; Snaith, H. J. Unravelling the Improved Electronic and Structural Properties of Methylammonium Lead Iodide Deposited from Acetonitrile. *Chem. Mater.* **2018,** *30* (21), 7737-7743.

(44) Bi, D.; Yang, L.; Boschloo, G.; Hagfeldt, A.; Johansson, E. M. Effect of Different Hole Transport Materials on Recombination in $CH_3NH_3PbI_3$ Perovskite-Sensitized Mesoscopic Solar Cells. *J. Phys. Chem. Lett.* **2013,** *4* (9), 1532-6.

(45) Bernechea, M.; Miller, N. C.; Xercavins, G.; So, D.; Stavrinadis, A.;

Konstantatos, G., Solution-processed solar cells based on environmentally friendly $AgBiS_2$ nanocrystals. *Nat. Photonics* **2016,** *10* (8), 521-525.

(46) Liu, Z.; Hu, J.; Jiao, H.; Li, L.; Zheng, G.; Chen, Y.; Huang, Y.; Zhang, Q.; Shen, C.; Chen, Q.; Zhou, H. Chemical Reduction of Intrinsic Defects in Thicker Heterojunction Planar Perovskite Solar Cells. *Adv. Mater.* **2017,** *29* (23), 1606774.